

A California Statewide Three-Dimensional Seismic Velocity Model from Both Absolute and Differential Times

by Guoqing Lin,^{*} Clifford H. Thurber, Haijiang Zhang,[†] Egill Hauksson, Peter M. Shearer, Felix Waldhauser, Thomas M. Brocher, and Jeanne Hardebeck

Abstract We obtain a seismic velocity model of the California crust and uppermost mantle using a regional-scale double-difference tomography algorithm. We begin by using absolute arrival-time picks to solve for a coarse three-dimensional (3D) P velocity (V_P) model with a uniform 30 km horizontal node spacing, which we then use as the starting model for a finer-scale inversion using double-difference tomography applied to absolute and differential pick times. For computational reasons, we split the state into 5 subregions with a grid spacing of 10 to 20 km and assemble our final statewide V_P model by stitching together these local models. We also solve for a statewide S -wave model using S picks from both the Southern California Seismic Network and USArray, assuming a starting model based on the V_P results and a V_P/V_S ratio of 1.732. Our new model has improved areal coverage compared with previous models, extending 570 km in the SW–NE direction and 1320 km in the NW–SE direction. It also extends to greater depth due to the inclusion of substantial data at large epicentral distances. Our V_P model generally agrees with previous separate regional models for northern and southern California, but we also observe some new features, such as high-velocity anomalies at shallow depths in the Klamath Mountains and Mount Shasta area, somewhat slow velocities in the northern Coast Ranges, and slow anomalies beneath the Sierra Nevada at midcrustal and greater depths. This model can be applied to a variety of regional-scale studies in California, such as developing a unified statewide earthquake location catalog and performing regional waveform modeling.

Online Material: Smoothing and damping trade-off analysis, *a priori* Moho depth, resolution tests, and map-view slices and cross sections through the 3D V_P and V_S models.

Introduction

Numerous studies of velocity structure in California have been done with varying scales in different areas (Table 1). The largest and most complete crustal tomography models in California are the recent southern California model by Lin *et al.* (2007) and the northern California model by Thurber *et al.* (2009). These studies have revealed key features of the crustal structure of California. The integration of the Northern and Southern California Seismic Networks (NCSN and SCSN) into a unified statewide network, the California Integrated Seismic Network (CISN; e.g., Hellweg *et al.*, 2007), has motivated the development of a statewide seismic velocity

model for locating earthquakes in California. In this study, we take advantage of the regional-scale double-difference (DD) tomography algorithm (Zhang and Thurber, 2006) to develop P - and S -wave velocity models for the entire state of California. Our P velocity model is derived from both first-arrival absolute and differential time picks obtained from the California seismic networks and has a horizontal grid spacing as fine as 10 km. The S velocity model is solved using the SCSN and USArray picks with a horizontal grid spacing of 30 km. There are numerous tomographic studies in California and it is impractical to compare our model with all of them; we focus on a comparison with the recent regional-scale tomographic studies for southern and northern California by Lin *et al.* (2007) and Thurber *et al.* (2009). Because our V_P and V_S models are solved using different sets of data and the V_P model has better resolution, we present

^{*}Now at Division of Marine Geology and Geophysics, Rosenstiel School of Marine and Atmospheric Science, University of Miami, Miami, Florida, 33149 (glin@rsmas.miami.edu).

[†]Also at Department of Geoscience, University of Wisconsin–Madison, 1215 W. Dayton St., Madison, Wisconsin 53706.

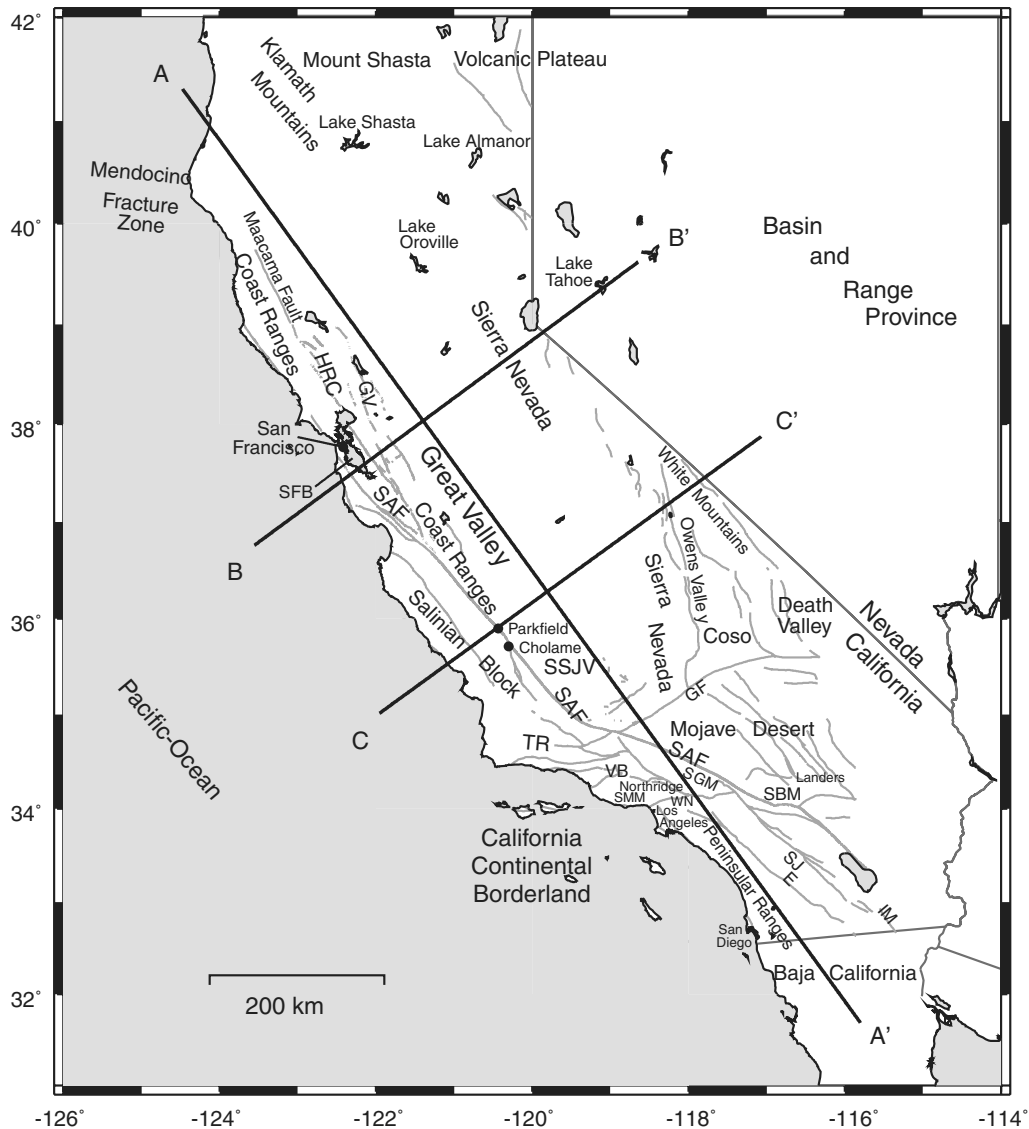


Figure 1. Map of selected geological and geographic features in our study area. The thick straight lines indicate the model cross sections shown in Figure 7. The NW–SE profile A–A' is parallel to the San Andreas fault, and the SW–NE profiles B–B' and C–C' are perpendicular to the San Andreas fault. Abbreviations: E, Elsinore fault; GF, Garlock fault; GV, Green Valley fault; HRC, Healdsburg–Rodgers Creek fault; IM, Imperial Valley fault; SAF, San Andreas fault; SBM, San Bernardino Mountains; SFB, San Francisco Bay; SGM, San Gabriel Mountains; SJ, San Jacinto fault; SMM, Santa Monica Mountains; SSJV, Southern San Joaquin Valley; TR, Transverse Ranges; VB, Ventura basin; WN, Whittier Narrows.

them separately with more emphasis on the V_P model. Figure 1 shows selected geological and geographic features in our study and the positions of three profiles for the velocity cross sections.

P-Wave Velocity Model

Data and Inversion Method

The data sets for our V_P model are the first-arrival absolute and differential times of 8720 earthquakes recorded by the seismic networks in California, consisting of 4325 events from the Northern California Seismic Network,

3668 events from the Southern California Seismic Network, and 727 events from the Pacific Gas and Electric seismic network (blue, pink, and green dots in Fig. 2a, respectively). These earthquakes were selected based on having the greatest number of P picks among those events within a 6 km radius, with a magnitude threshold of 2.5. The total number of P picks in our data set is 551,318 with an average of 63 picks per event. In order to improve constraints on the shallow crustal structure, we assembled first-arrival times from 3110 explosions and airguns (red circles in Fig. 2b) recorded on profile receivers and network stations. The principal active-source data sets and sources are listed in Table 2.

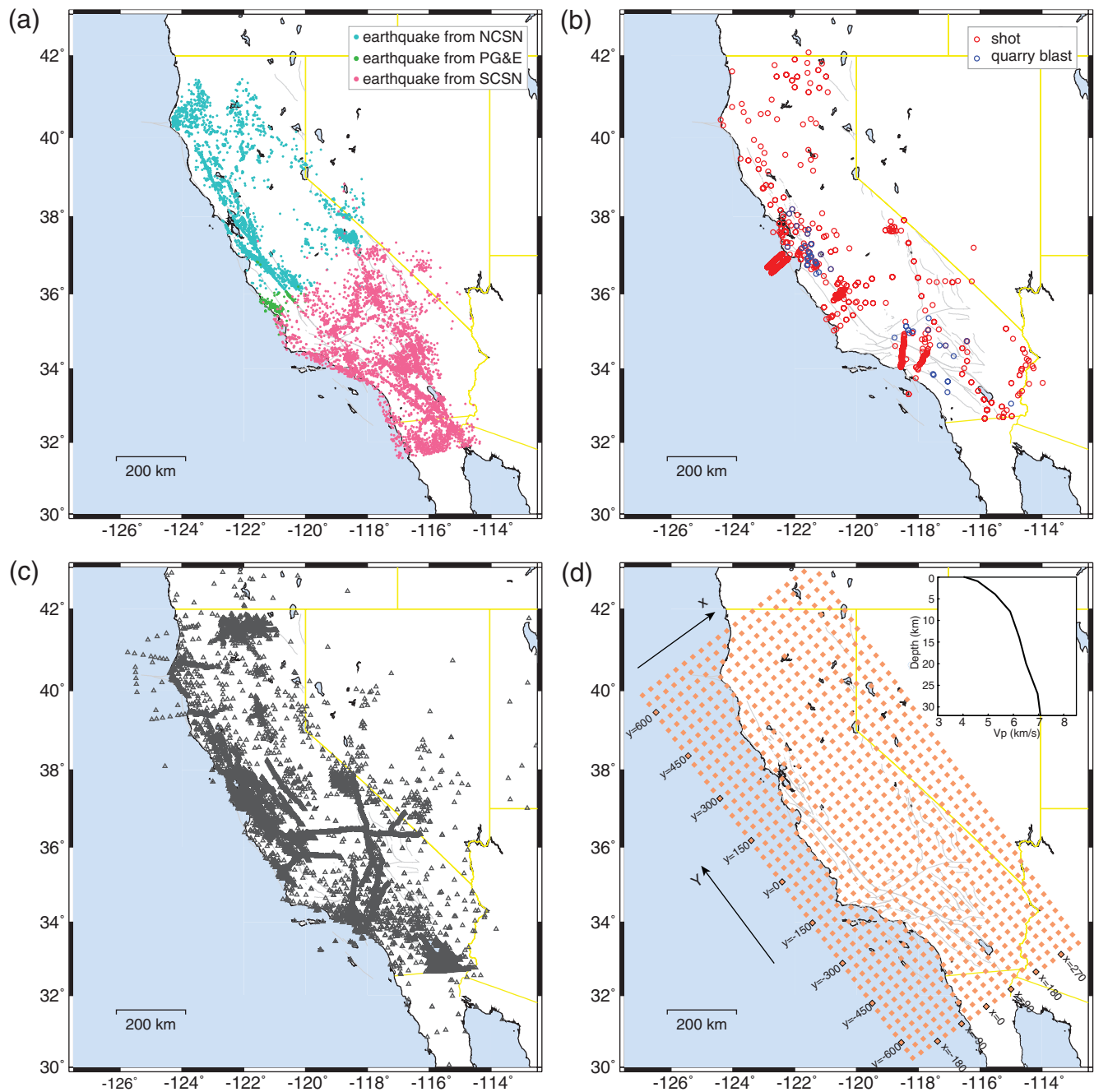


Figure 2. Event and station distributions in our study area and starting inversion grid nodes for the 3D coarse model (30-km horizontal spacing). (a) earthquakes; (b) controlled sources; (c) stations; (d) inversion grid nodes (small panel shows the 1D starting velocity model).

Quarry blasts, which have known locations but unknown origin times, are also valuable to be included in tomographic inversions because they provide constraints that are almost as good as the active-source data. We include data from 44 quarry blasts (blue circles in Fig. 2b), with 19 in southern California (see Lin *et al.*, 2007) and 25 in northern California. Figure 2c shows the locations of temporary and network stations used in our study.

The model presented in this study is obtained by using a regional-scale DD tomography algorithm (tomofDD; Zhang

and Thurber, 2006), which is a generalization of DD location (Waldhauser and Ellsworth, 2000). It maps a spherical-Earth coordinate system into a Cartesian coordinate system (a sphere in a box; Flanagan *et al.*, 2007) and incorporates a finite-difference travel time calculator and spatial smoothing constraints. This algorithm is designed to solve jointly for 3D velocity structure and earthquake locations using both first-arrival times and differential times, leading to improved resolution in the seismically active areas where the differential data provide dense sampling.

Table 1

A Subset of the Previous Studies on Seismic Velocity Structure in California

Study Area	References
Coalinga	Eberhart-Phillips (1990)
Coast Ranges	Eberhart-Phillips (1986); Henstock <i>et al.</i> (1997); Bleibinhaus <i>et al.</i> (2007)
Coso geothermal area	Hauksson and Unruh (2007)
Coyote Lake	Thurber (1983)
Great Valley	Hwang and Mooney (1986); Godfrey <i>et al.</i> (1997)
Greater Los Angeles basin	Magistrale <i>et al.</i> (1996); Hauksson and Haase (1997); Lutter <i>et al.</i> (1999)
Loma Prieta	Foxall <i>et al.</i> (1993); Thurber <i>et al.</i> (1995); Eberhart-Phillips and Michael (1998)
Monterey Bay	Begnaud <i>et al.</i> (2000)
Parkfield region	Eberhart-Phillips and Michael (1993); Thurber <i>et al.</i> (2003, 2006)
San Francisco Bay region	Manaker <i>et al.</i> (2005); Hardebeck <i>et al.</i> (2007); Thurber <i>et al.</i> (2007)
Santa Monica Mountains	Lutter <i>et al.</i> (2004)
Sierra Nevada arc	Brocher <i>et al.</i> (1989); Fliedner <i>et al.</i> (1996, 2000); Boyd <i>et al.</i> (2004)
Entire southern California	Hauksson (2000); Huang and Zhao (2003); Zhou (2004)

3D Coarse Model

Because of the large spatial scale and amount of data in our study, we first solve for a coarse 3D V_p model starting with a one-dimensional (1D) velocity model (shown in the small panel of Fig. 2d) for the entire state. This 1D model is based on standard regional 1D velocity models used to locate earthquakes by the seismic networks in northern and southern California. The starting model nodes (shown in Fig. 2d) are uniformly spaced at 30 km intervals in the horizontal directions and extend 570 km in the SW–NE direction and 1320 km in the NW–SE direction. In the vertical direction, the nodes are positioned at $-1, 1, 4, 8, 14, 20, 27, 35,$ and 45 km (relative to mean sea level). We only use

absolute arrival times for this 3D coarse model. An *a priori* Moho is not included at this stage, but is introduced later for the finer-scale model. Preliminary inversions were carried out using the tomography algorithm simul2000 (Thurber and Eberhart-Phillips, 1999). This algorithm simultaneously solves for 3D velocity structure and earthquake locations using the first-arrival times employing an iterative damped-least-squares method. This step was taken for data quality control purposes (i.e., identifying poorly constrained events and picks with very high residuals), and to provide formal but approximate estimates of velocity model resolution and uncertainty. After the data quality control step using simul2000, we applied the regional-scale DD tomography algorithm, which is more suitable for the large-scale area

Table 2

Active-Source Data Sets Included in the Statewide Tomographic Inversion

Experiment Name	Reference	Year	No. Shots	No. Stations
USGS	Warren (1978)	1967	9	147
Geysers-San Pablo Bay	Warren (1981)	1976	5	135
Oroville	Spieth <i>et al.</i> (1981)	1977	5	118
Imperial Valley	Kohler and Fuis (1988)	1979	41	932
Western Mojave Desert	Harris <i>et al.</i> (1988)	1980	10	245
Gilroy-Coyote Lake	Mooney and Luetgert (1982)	1980/1981	4	236
Livermore	Williams <i>et al.</i> (1999)	1980/1981	3	251
Great Valley	Murphy (1989); Colburn and Walter (1984)	1981/1982	7	221
San Juan Bautista	Mooney and Colburn (1985)	1981/1982	6	335
Shasta 1981	Kohler <i>et al.</i> (1987)	1981	1	274
Shasta 1982	Kohler <i>et al.</i> (1987)	1982	9	299
Morro Bay	Murphy and Walter (1984)	1982	9	230
Coalinga	Murphy and Walter (1984)	1983	9	209
Long Valley	Meador <i>et al.</i> (1985)	1983	9	278
San Luis Obispo	Sharpless and Walter (1988)	1986	10	123
Loma Prieta	Brocher <i>et al.</i> (1992)	1990	2252	16
San Francisco Bay 1991	Murphy <i>et al.</i> (1992); Kohler and Catchings (1994); Brocher and Pope (1994)	1991	6	300
PACE 1992	Fliedner <i>et al.</i> (1996)	1992	5	384
Southern Sierra	Fliedner <i>et al.</i> (1996)	1993	23	1241
San Francisco Bay 1993	Catchings <i>et al.</i> (2004)	1993	14	399
LARSE 1994	Murphy <i>et al.</i> (1996)	1994	125	889
LARSE 1999	Fuis, Murphy, <i>et al.</i> (2001)	1999	78	925
Parkfield	Thurber <i>et al.</i> (2003, 2004); Hole <i>et al.</i> (2006)	2003	157	242
Network	Northern and Southern California Earthquake Data Center	1976–2003	270	659

in this study. To make the inversion more stable, some regularization method is required, such as smoothing and damping. Smoothing regularization provides a minimum-feature model that contains only as much structure as can be resolved above the estimated level of noise in the data (Zhang and Thurber, 2003). Damping and smoothing are often selected empirically, by running a series of single-iteration inversions with a large range of values, and plotting the data variance versus model variance trade-off curves (e.g., Eberhart-Phillips, 1986, 1993). We explored a wide range of damping (from 25 to 1000) and smoothing (from 0 to 1000) to make sure that we looked at the entire trade-off curve instead of a portion of it. The smoothing constraint weighting of 100 (same for the horizontal and vertical directions) and the damping parameter of 350 were chosen by examining these trade-off curves, which produced good compromises between data misfit and model variance (see ⑤ Figure S1 in the electronic edition of BSSA).

3D Starting Model Adjustments

Our preliminary modeling work did not include an *a priori* velocity increase at the Moho, but first-arrival body-wave tomography by itself was not capable of imaging sharp discontinuities. Thus, after we obtained the 3D coarse velocity model, we introduced an *a priori* Moho interface (see ⑤ Figure S2 in the electronic edition of BSSA) from the results of Fuis and Mooney (1990), which was a modification of Mooney and Weaver (1989). We set the velocity to 8 km/sec in the model layer right below the Moho and 8.2 km/sec at the

deepest layer with a linear gradient for the layers between these two layers. In order to start with a conservative 3D model, we removed the low-velocity anomalies in the 3D coarse model, that is, we require that velocity is initially a monotonically increasing function of depth. The resulting adjusted 3D model is the starting model for our final *P* velocity model. Figure 3a shows the map view of this model at 4 km depth, with the layer-average velocity values in the inset of Figure 3b. In order to check the effects of the inclusion of the Moho interface on our final results, we compared our final model with a model obtained without a Moho (low-velocity anomalies are still removed). The two models are quite similar over well-resolved areas and the model differences between the initial models are reduced after the inversion, indicating that our process converges. ⑤ Table S1 in the electronic edition of BSSA shows a comparison of models with and without the inclusion of a Moho interface.

In order to use differential times to obtain a finer-scale model given our computer memory limitations, we split the entire state into five subregions (Fig. 3a). The adjacent subregions overlap by about 30 km. We use the same depth layers as the coarse model. Figure 3b shows the event and station distributions for subregion 1 as an example. For each subregion inversion, we use absolute and differential times from events inside the subregion (blue circles in Fig. 3b) that are recorded by all the stations (black triangles) and only absolute times from events outside of the subregion (pink circles) that are recorded by stations inside of the subregion. In this way, we improved the resolution of the resulting velocity model for

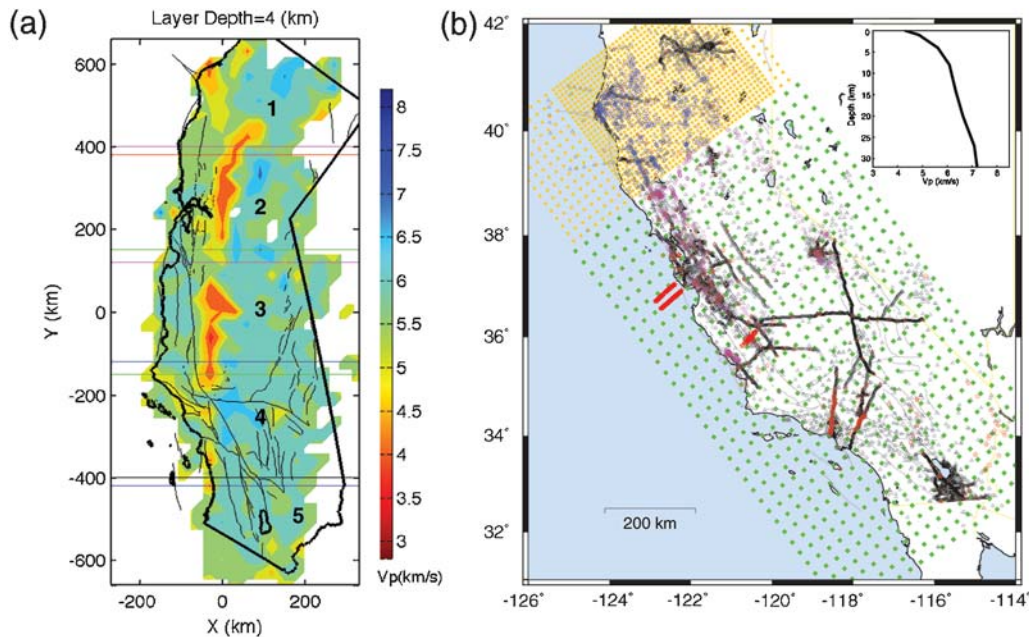


Figure 3. (a) Map view of the 3D coarse velocity model at 4 km depth and the boundaries of the 5 subregions. (b) Event and station distribution in the subregion 1 (small panel shows the 1D layer-average velocity). Yellow squares: finer inversion nodes inside of subregion; green squares: nodes with fixed velocities; blue circles: earthquakes inside of subregion 1; pink circles: earthquakes outside of subregion 1 but recorded by stations inside of the subregion; black triangles: permanent and temporary stations; red stars: active sources (shots and quarry blasts). Please refer to the text for more details.

the deeper layers due to the inclusion of substantial data at large epicentral distances. We also include all available explosion and quarry data for each subregion (red stars). Inside of each subregion, the horizontal nodes are spaced at 10 km intervals in the areas with dense data coverage and 20 km in other areas (yellow squares). The node spacing outside of each subregion is 30 km from the coarse model (green squares). The initial velocity value at each node is computed from the velocity values at the surrounding eight nodes of the coarse initial model using trilinear interpolation as described in [Thurber and Eberhart-Phillips \(1999\)](#). The velocities outside of each subregion are fixed during the inversion of the inside-subregion velocities. We inverted five local models separately; our final statewide velocity model is a stitched version of all the five subregion models. The velocities in the areas of overlap are computed as the average velocities of the two adjacent subregions. In order to test the robustness of our stitching approach, we inverted a model that includes subregions 1 and 2 and compared the resulting model with the stitched model. The two models are quite similar with some minor differences that are likely caused by different regularization parameters, which are determined individually for each inversion by examining data variance versus model variance trade-off curves.

Model Quality and Resolution

The quality of our model can be evaluated by its ability to (1) fit the observed arrival-time data, and (2) produce accurate locations for onland controlled-source explosions that have known coordinates. Figure 4 shows a comparison of the arrival-time residual distribution before (a) and after the coarse (b) and final (stitched) (c) 3D velocity inversions for the entire data set (including controlled sources). The root-mean-square (rms) misfit is reduced by over a factor of 3, from 1.26 sec to 0.37 sec, after the 3D coarse model inversion, and then to 0.32 sec after the final model inversion. The reason that the fit to absolute times in the subregion model inversions is only slightly better than the coarse model fit is because the purpose of this step is to improve fine-scale velocity resolution by using differential times. A hierarchical weighting scheme is applied with greater weight to the absolute data for the first two iterations and greater weight to the differential data for the next four iterations. Note that most of the improvement of arrival-time fit after the 3D final model inversion is mainly due to the lower differential time residuals, where the rms misfit of the differential times is reduced from 0.28 sec to 0.11 sec.

We independently located the onshore explosions using the starting 1D and the coarse and final 3D velocity models and then calculated the horizontal and vertical location differences between the relocations and the known true locations. Figure 5 shows histograms of shot location accuracy relocated using the starting 1D model compared with the two 3D models for both horizontal and vertical coordinates. The horizontal location errors are all positive; the vertical errors

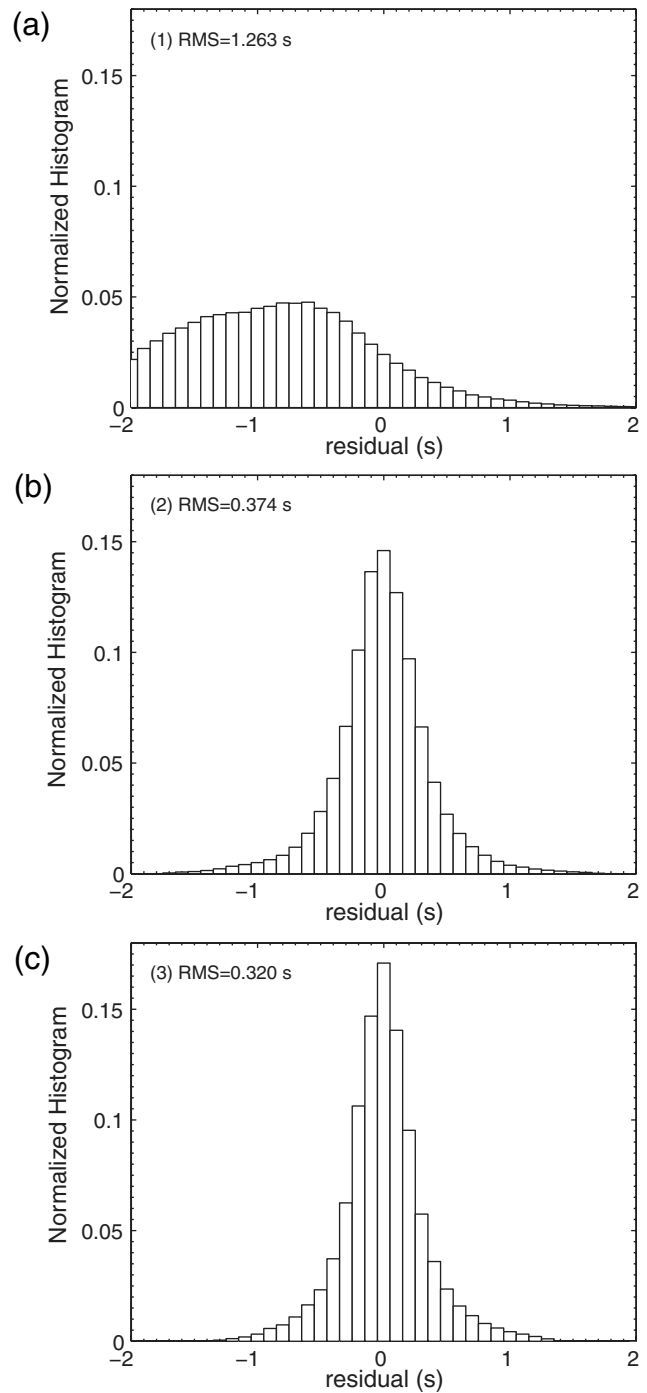


Figure 4. The arrival-time residual distribution for the entire data set (including controlled sources) (a) before 3D velocity inversion; (b) after 3D coarse model inversion; (c) after 3D final model inversion.

are positive when the assigned location is deeper than the true location and negative when the assigned location is shallower than the true location. For the 1D model, the error distributions are quite broad, with a mean error of 1.23 km, and a standard deviation of 1.08 km horizontally. The vertical error distribution has peaks at about 0.6 and 4.5 km, a mean (absolute) error of 2.19 km, and a standard deviation of

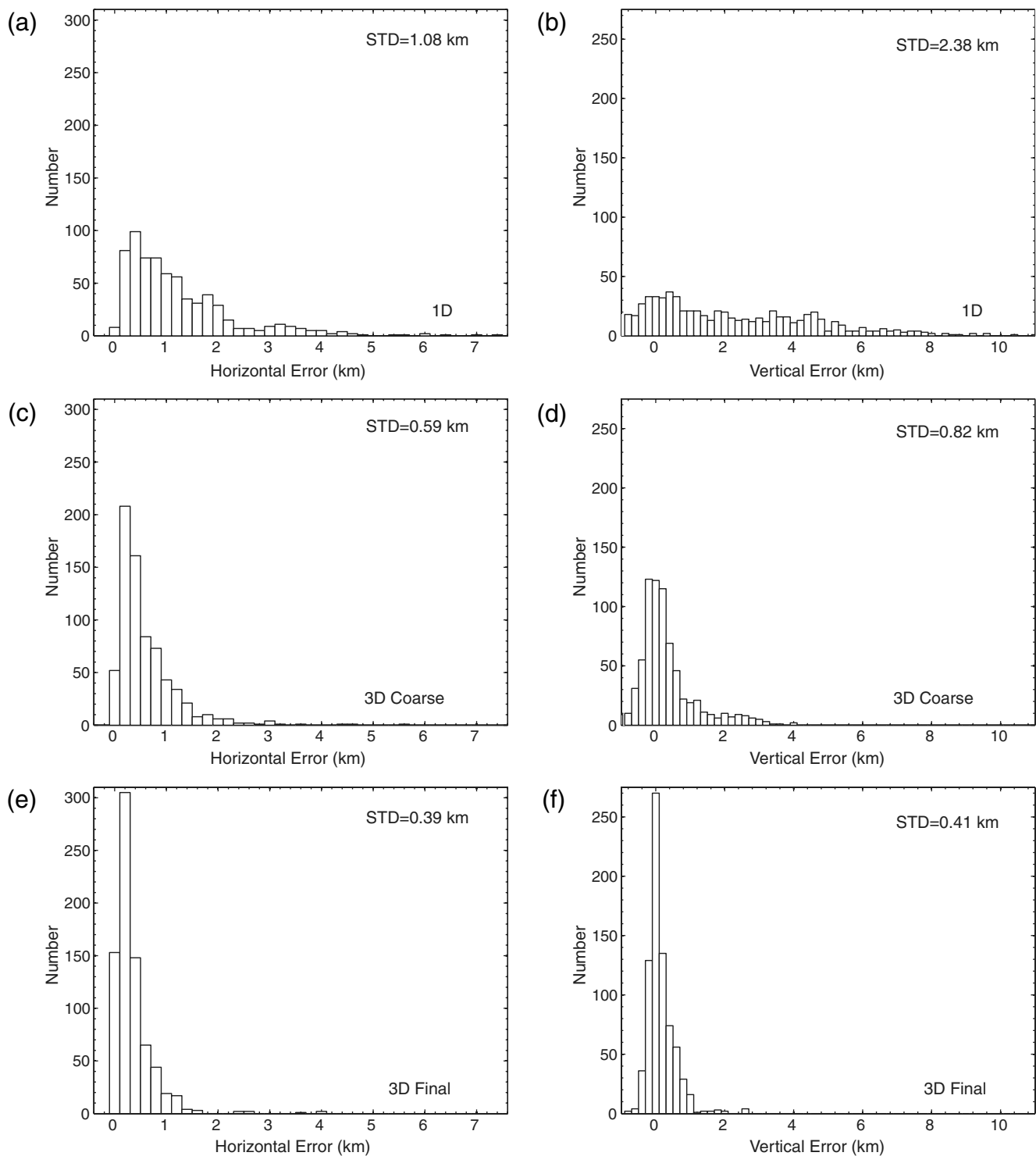
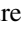



Figure 5. Histograms of the differences between relocations and known true locations for onland explosions. The two columns are for horizontal and vertical location errors, respectively. (a) and (b) 1D model; (c) and (d) 3D coarse model; (e) and (f) 3D final model.

2.38 km. In contrast, the 3D coarse model error distributions are peaked between 0 and 1 km, with mean errors of 0.60 and 0.32 km, and standard deviations of 0.59 and 0.82 km for the horizontal and vertical errors, respectively. Although this model is coarse, the 3D shot relocations are significantly improved, especially in depth. This is because a single

1D-velocity model cannot account for lateral heterogeneity in velocity structure across all of California. Further, the 3D final model location error distributions are peaked around 0.2 km, with mean errors of 0.35 and 0.15 km and standard deviations of 0.39 and 0.41 km for the horizontal and vertical errors, respectively. The poorly located shots fall into several

categories. One group is distant shots recorded on permanent network stations for cases in which we were not able to obtain the corresponding refraction profile picks. An example is the shots from the PACE 1992 project (Fliedner *et al.*, 1996). Others are cases for which data for a particular shot were split into two separate events, due to the fact that the data were obtained and entered into the database separately. Examples are a number of shots from the Parkfield area and several LARSE shots. Finally, there are a few shots for which only profile picks are available, and the recording geometry is too poor to constrain the locations adequately. The reduction in relocation errors of about a factor of 2 over the 3D coarse model indicates that our final model significantly improves resolution for the lateral heterogeneities in the 3D velocity structure, especially at shallow depths.

To assess the model quality, we performed a restoration and a checkerboard resolution test similar to those in Thurber *et al.* (2009). In the restoration test, event hypocenters, station locations, and synthetic travel times, calculated from the final inverted model, have the same distribution as the real data. We followed the same inversion strategies as those for the real data and examined the recovering ability of our algorithms. The inverted final model is similar to the true model over well-resolved areas (see  Figure S3 in the electronic edition of *BSSA*). In the checkerboard test, the synthetic times are computed through the 1D starting velocity model with $\pm 5\%$ velocity anomalies across three grid nodes. The results are shown in Figure S4 (see the  electronic edition of *BSSA*). Note that in this test, we did not include the Moho interface, but still removed low-velocity anomalies as was done for the real data inversion. Some smearing is still seen, part of which is likely due to the interpolation of velocities when obtaining the starting velocities for subregion models.

Final *P*-Wave Velocity Model

Map Views. Figure 6 shows map view slices through the resulting tomographic *P* velocity model. Pink dots in each figure represent earthquakes relocated within ± 1 km of each layer depth. The white contours enclose the areas where the derivative weight sum (DWS; Thurber and Eberhart-Phillips, 1999) is greater than 300. Derivative weight sum measures the sampling of each node and serves as an approximate measure of resolution (Zhang and Thurber, 2007). Areas with DWS values above 300 correspond to well-resolved areas in the synthetic tests. In the following, we show average velocities at each layer computed for these areas. In order to quantitatively compare our model with previous tomography models, we interpolated the southern and northern California models by Lin *et al.* (2007) and Thurber *et al.* (2009) onto our inversion grids and calculated the correlation coefficients at each layer depth. We will refer to these two models as the SC and NC models in the following.

Figure 6a,b shows the *P*-wave velocities in the top two layers of our model. The average velocity values are 5.26 km/sec at 1 km and 6.0 km/sec at 4 km depth. The ve-

locities in these shallow layers generally correlate with the surface geology. Lower values are observed in basin and valley areas, such as the Great Valley, southern San Joaquin Valley, Ventura basin, Los Angeles basin, and Imperial Valley, whereas relatively higher velocities are present in the mountain ranges, such as the northern Coast Ranges, Transverse Ranges, Peninsular Ranges, and Sierra Nevada. The correlation coefficients for the well-resolved areas of these two layers between our model and the NC model are 0.49 and 0.56, respectively. The relatively low correlations for these two layers are mainly due to the low-velocity anomalies in the Great Valley and fast anomalies in the Sierra Nevada in our model. The lowest velocity anomalies (about 2.9 km/sec) appear in the Great Valley and southern San Joaquin Valley. However, these slow anomalies are at the edge of our well-resolved areas because of the sparse event distribution in this region. Fairly high-velocity anomalies (~ 6.0 km/sec) at 1 km depth in the Klamath Mountains and Mount Shasta area are observed that are consistent with the results from seismic-refraction and gravity data in this area (Zucca *et al.*, 1986; Fuis *et al.*, 1987), but are not seen in the recent northern California *P*-wave velocity model by Thurber *et al.* (2009). This high-velocity body extends to 14 km depth in our model, reaching ~ 6.5 – 6.7 km/sec at 4 km, ~ 6.7 – 7.1 km/sec at 8 km, and ~ 7 – 7.1 km/sec at 14 km depth, with relatively little structural variations along the north-south direction. These velocities are consistent with the conclusion by Fuis *et al.* (1987), who argued that an imbricated stack of oceanic rock layers underlies the Klamath Mountains. Another high-velocity anomaly zone is apparent at 1 and 4 km depth in the Lake Oroville area. The ~ 6.8 km/sec velocity at 4 km depth is generally consistent with the observations by Spieth *et al.* (1981) that the velocity is of the order of 7.0 km/sec at a depth of 5 km. This high-velocity anomaly (~ 6.9 km/sec) extends to 8 km depth in our model. The high velocities at 1 km depth in the southern Sierra Nevada area, ranging from 5.2 km/sec to 5.8 km/sec, are consistent with the results of Fliedner *et al.* (1996, 2000). The velocities at 4 km depth are generally higher than those estimated by Thurber *et al.* (2009) (~ 6.0 km/sec compared with ~ 5.3 km/sec); our model is more consistent with the results based on the active seismic refraction experiment by Fliedner *et al.* (1996, 2000).

In southern California, the correlation coefficients for these two layers between our model and the SC model are 0.65 and 0.56, respectively. Note that these coefficients are computed over the resolved areas in the model of Lin *et al.* (2007), corresponding to the area of $X = -100$ to 200 km and $Y = -620$ to -100 km. Near-surface velocities in our model are also relatively high in the western Mojave Desert in our model. The anomalies are slightly higher than previous results (e.g., Hauksson, 2000; Lin *et al.*, 2007). We think this may be due to the inclusion of the active-source data in this area, which were not used before. In the Imperial Valley area, the slowest velocity at 1 km depth is 3.07 km/sec in this study, but about 3.6 km/sec at the surface in Lin *et al.* (2007), who concluded that their model slightly overestimates

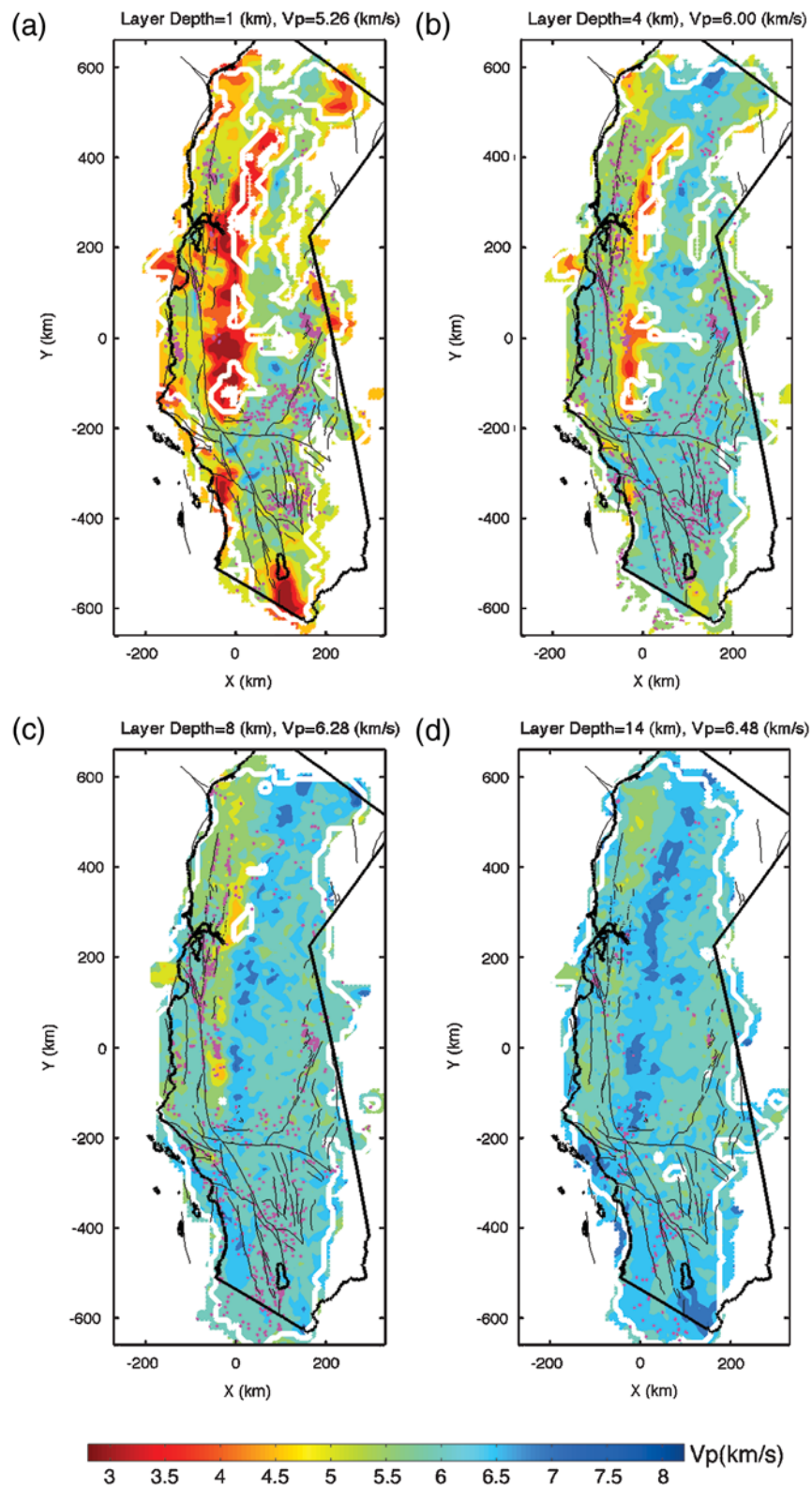


Figure 6. Map views of the P -wave velocity model at different depth slices. The white contours enclose the areas where the derivative weight sum is greater than 300. The average velocities are computed over these areas. Pink dots represent relocated earthquakes. Black lines denote coast line and lakes, gray lines rivers and surface traces of mapped faults. (Continued)

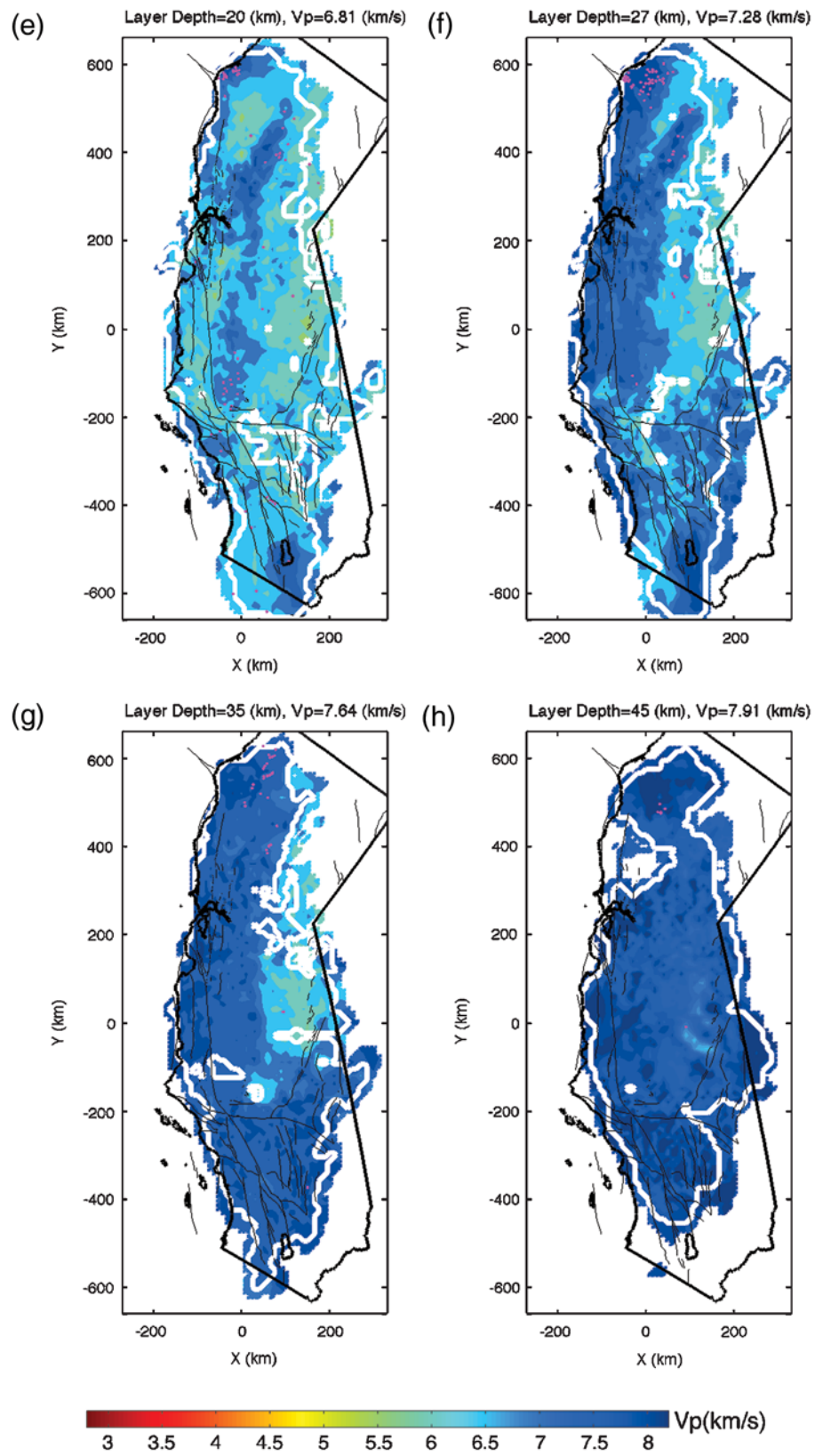


Figure 6. Continued.

the near-surface velocity compared with seismic refraction results (Fuis *et al.*, 1984). The reduction of this overestimation indicates that our model has better resolution for near-surface structure. The southern San Joaquin Valley is better resolved in this new model, which is at the northern boundary of the study area in Lin *et al.* (2007).

Figure 6c,d shows map views for 8 and 14 km depths, with average velocity values of 6.26 km/sec and 6.46 km/sec, respectively. These layers are the two best-resolved layers in our model because of the abundant seismicity at these depths, and the results are generally quite compatible with previous tomographic results. At 8 km depth, a strong velocity contrast is apparent between the Great Valley and the Sierra Nevada. At 14 km depth, some of the features we imaged for the shallow layers are reversed, that is, the basin and valley areas show relatively high-velocity anomalies and lower values are present under the mountain ranges. The reversal of the velocity anomalies associated with most of the major basins is also observed in previous southern and northern California tomography studies (Lin *et al.*, 2007; Thurber *et al.*, 2009). The correlation coefficients for these two layers between our model and the NC model are 0.61 and 0.47, and 0.35 and 0.49 with the SC model, respectively. The relatively poor correlation with the NC model is mainly due to the slower velocities ($\sim 5\%$) in the northern Coast Ranges than what is observed in the Thurber *et al.* (2009) model. The correlation coefficients with the SC model are reduced compared with the shallower layers. For these two layers, our model is generally faster than the Lin *et al.* (2007) model by about 5% in the basin areas, such as the Ventura basin, Los Angeles basin, and Imperial Valley.

Map views for the 20 and 27 km depth layers are shown in Figure 6e,f, with average velocity values of 6.81 km/sec and 7.28 km/sec, respectively. The correlation coefficients for these two layers between our model and the NC model are 0.65 and 0.72, respectively. The resolution of the southern California model by Lin *et al.* (2007) is poor below 17 km depth, so we focus on the comparison in northern California. At 20 km depth, the model is consistent with

the results of Thurber *et al.* (2009), but is slightly slower in the center of the Great Valley. At 27 km depth, the Sierra Nevada area shows about 6.0 km/sec low-velocity anomalies, but in the same area, the velocity in Thurber *et al.* (2009) is about 6.5 km/sec. Our model extends to 45 km depth. Figure 6g,h shows the map views of the last two layers at 35 km and 45 km depths. Although the model is not resolved nearly as well as the shallower layers, we are able to see the low-velocity anomalies in the Sierra Nevada region; the correlation coefficients for these two layers between our model and the NC model are 0.70 and 0.46, respectively.

Cross Sections. We present three cross sections to illuminate the large-scale features of the model. One is parallel to the San Andreas fault (SAF; $X = 0$ km in the Cartesian coordinate system), and the other two are perpendicular to the SAF ($Y = 210$ km and $Y = -30$). A complete set of cross sections is provided in the electronic edition of BSSA. In Figure 7 we show the velocity cross sections through the resulting model along the three profiles whose locations are shown in Figure 1.

The $X = 0$ km section in Figure 7a starts in the northern Coast Ranges where intermediate velocities ($V_p < 6.2$ km/sec) extend into the lower crust. At depths greater than 20 km, the seismicity and high velocities of the subducting Gorda Plate are visible. From $Y \sim 350$ to -210 km, the low near-surface velocities of the Great Valley and southern San Joaquin Valley sediments and sedimentary rocks are evident, extending to depths of ~ 10 km in the northwest and to ~ 4 km in the southeast. High-velocity rocks ($V_p \sim 6.5$ km/sec) of the underlying Great Valley ophiolite body are present throughout this part of the section. The section crosses the Garlock fault ($Y \sim -210$ km) and the SAF ($Y \sim -255$ km), where upper and midcrustal velocities are relatively low ($V_p < 6.3$ km/sec), and then cuts through the San Gabriel Mountains (SGM) and Peninsular Ranges where the upper crust velocities are relatively high ($V_p > 6.2$ km/sec) at shallow depths. Beneath the SAF and SGM, a strong low-velocity zone is apparent, as identified in

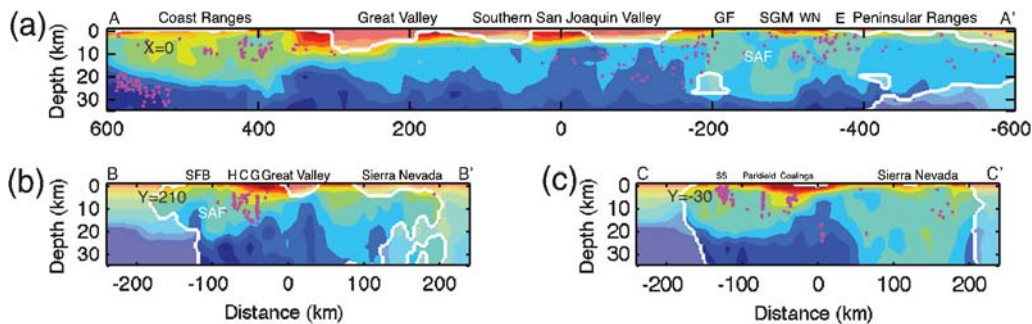


Figure 7. Cross sections of the absolute P -wave velocity along the three profiles shown in Figure 1. Again, the pink dots represent relocated earthquakes and the white contours enclose the area where the derivative weight sum is less than 300. Color scale is the same as in Figure 6. Abbreviations: C, Calaveras fault; E, Elsinore fault; GF, Garlock fault; G, Greenville fault; H, Hayward fault; SAF, San Andreas fault; SFB, San Francisco Bay; SGM, San Gabriel Mountains; SS, San Simeon; WN, Whittier Narrows.

previous studies in this area, which has been interpreted to indicate fluids (e.g., [Ryberg and Fuis, 1998](#); [Fuis et al., 2000](#)).

The section in [Figure 7b](#) cuts across the seismically quiet southern San Francisco (SF) Peninsula and SF Bay ($X = -120$ to -90 km) and then reaches the seismically active Hayward, Calaveras, and Greenville faults beneath the East Bay ($X = -70$ to -30 km). The section then enters the Great Valley, where the high-velocity basement, thought to be ophiolite (e.g., [Godfrey et al., 1997](#)), shallows to the northeast ($X = -30$ to $+50$ km). After that, the section enters the Sierra Nevada where a thicker crust with a velocity of ~ 6.2 km/sec extends to 32 km depth. The section in [Figure 7c](#) passes through the seismic activity of San Simeon ($X = -120$ km), Parkfield ($X = -75$ km), and Coalinga ($X = -30$ km). Even with the 10 km model gridding, the velocity contrast across the San Andreas at Parkfield is evident (southwest side faster, e.g., [Thurber et al., 2006](#)). In this section as well, the high-velocity Great Valley ophiolite body is evident with a predominantly southwestern dip of its upper surface, consistent with potential field data ([Jachens et al., 1995](#)). At $X \sim 50$ km, we see a transition to the slower, thicker crust of the Sierra Nevada.

S-Wave Velocity Model

Although S -wave velocity models in northern California are available from ambient noise and surface wave data (e.g., [Yang et al., 2008](#)), there is no 3D model based on regional network data. In this study, we use the S first-arrival times from the SCSN and USArray to solve for a V_S model. Note that these data are different from those used for the V_P model. [Figure 8a](#) shows the 1020 SCSN and 1292 USArray events with at least 4 P and 4 S picks. Due to the sparse distribution of the data, we use the velocity inversion nodes of the 3D coarse V_P model (i.e., 30 by 30 km horizontal node spacing). The starting S velocities are derived from our resolved V_P model and a constant V_P/V_S of 1.73. The resolution estimated by the DWS values is quite poor. In order to test the robustness of the S model, we also start with the S velocity values from the ambient noise and teleseismic multiple-plane-wave tomography results by [Yang et al. \(2008\)](#). The well-resolved part agrees with the results starting with the constant V_P/V_S , indicating that the model is relatively robust. [Figure 8b](#) shows the map view of our resolved V_S model at 8 km depth. The white contours enclose the area where the derivative weight sum is greater than 100. We also compared our V_P and V_S models to the empirical $V_P - V_S$

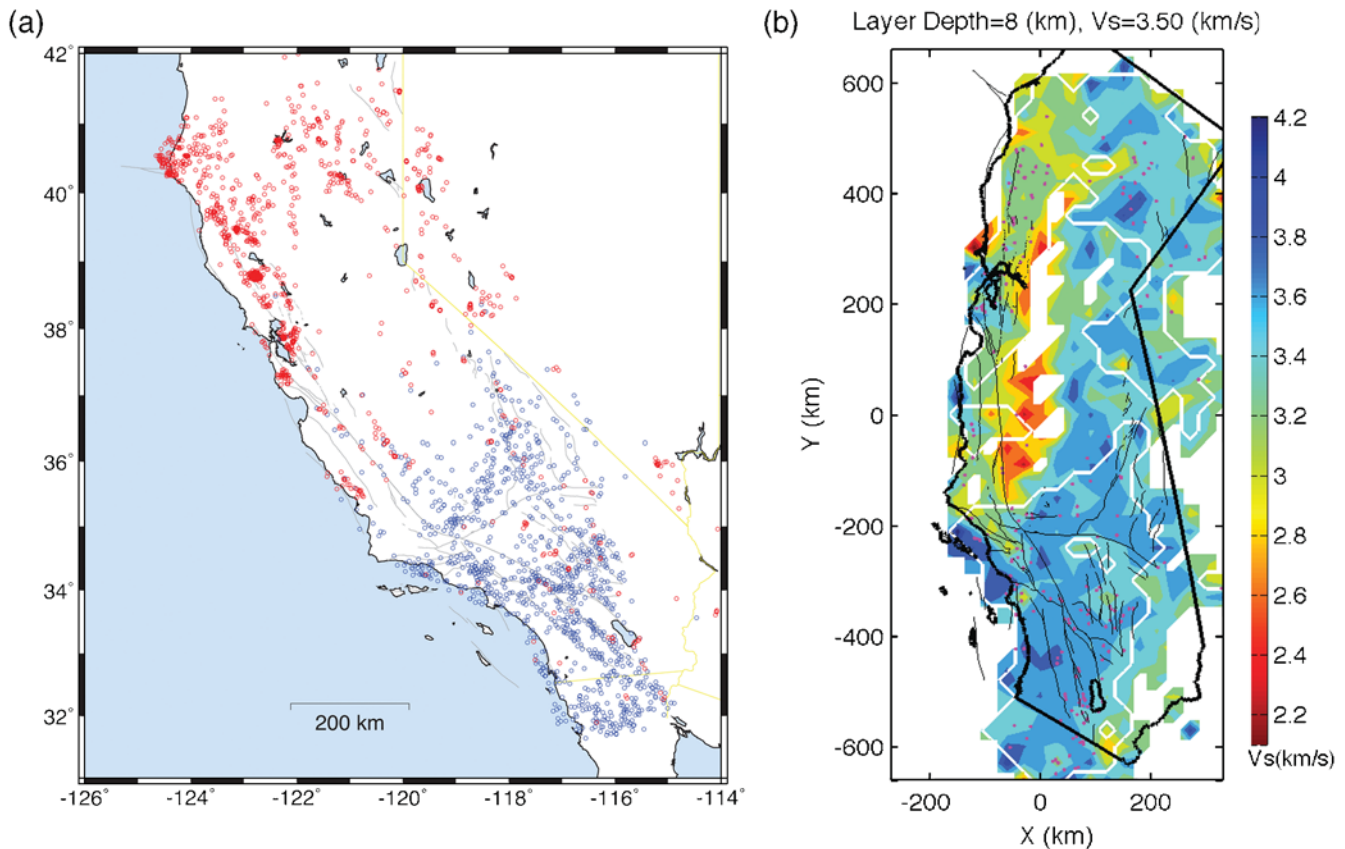



Figure 8. (a) Event distribution for V_S model. The red and blue circles represent the events from the USArray and SCSN, respectively. (b) Map view of our resolved V_S model at 8 km depth. Areas where the derivative weight sum is greater than 100 are shown. The average velocity is computed over these areas. The pink dots represent relocated earthquakes.

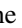
relation of Brocher (2005). This relation is derived from a diverse dataset, including wireline borehole logs, vertical seismic profiles, laboratory measurements, and seismic tomography models, and can be used to infer V_S for the entire Earth's crust from V_P . Using the layer-average P velocities as inputs, we obtained the corresponding empirical S velocities. Our comparison indicates that the tomography-based V_S results are faster than predicted by the empirical relation at 1 and 35 km depth, and lower than expected at 8 km depth. Due to the poor resolution of this model, we do not attempt to solve for Poisson's ratio and other parameters that depend on V_P/V_S values. A complete set of map views and cross sections of our S -wave model is provided in the  electronic edition of *BSSA*.

Discussion

Our model is the first 3D seismic velocity model for the entire state of California based on local and regional arrival-time data. It has improved areal coverage compared with the previous northern and southern California models, and extends to greater depth due to the inclusion of substantial data at large epicentral distances. The combination of northern, southern, and central California data sets results in better-resolved velocity structure at the study boundaries of previous tomographic models, such as the San Joaquin Valley and southern Sierra Nevada. Because of the 10 km horizontal grid spacing in our model inversion, which is larger than the distance cutoff of most waveform cross-correlation calculations (≤ 5 km), we did not apply any differential times from cross-correlation in this study. There may be some finer-scale structures that are not resolved due to the data and grid spacing used in our model. We compared our model with some results based on refraction and/or reflection data. Our model generally agrees with most of the studies, such as in the Diablo and Gabilan Ranges (Steppe and Robert, 1978; Walter and Mooney, 1982), the Coyote Lake (Mooney and Luetgert, 1982), the Long Valley (Luetgert and Mooney, 1985), the San Francisco Bay area (Holbrook *et al.*, 1996), the southern Sierra (Fliedner *et al.*, 1996), and the Mojave Desert (Fuis, Ryberg, *et al.*, 2001); but slightly overestimates near-surface velocity values in some basins and valleys, such as in the Imperial Valley (McMechan and Mooney, 1980; Fuis *et al.*, 1984), the Great Valley (Colburn and Mooney, 1986), the Livermore area (Meltzer *et al.*, 1987), and the greater Los Angeles basin (Fuis, Ryberg, *et al.*, 2001b).

The differences between this statewide velocity model and previous regional-scale models are due to several factors, such as data sets, grid spacing (cell size), tomographic algorithms, and inversion parameters (e.g., damping, smoothing, and residual weighting). The model is very similar to the recent northern California model by Thurber *et al.* (2009) for the middle to lower crust because the two studies use the same type of data sets (both absolute and differential times) and inversion algorithm (tomofDD), whereas the southern California model by Lin *et al.* (2007) is derived

by applying the SIMULPS algorithm (Thurber, 1983, 1993; Eberhart-Phillips, 1990; Evans *et al.*, 1994) to absolute arrival times for composite events. We also calculated the correlation coefficients, which are 0.67, 0.56, 0.36, 0.54, and 0.69 for the top five layers, between our model and the SCEC unified velocity model (Version 4, Magistrale *et al.*, 2000). Note that the SCEC model is based on geotechnical borehole seismic velocity data and the regional tomographic model of Hauksson (2000), which is also obtained by applying the SIMULPS algorithm. The slightly better correlation at 1 km depth is due to the low-velocity anomalies in the basin areas. Our new model is generally consistent with these previous results. The improved resolution of our model in near-surface layers over the previous California tomographic models is mainly due to the large amount of active-source data in this study.

The goal of this study is not to replace the previous tomographic models in California that have more detail than can be resolved by our data and grid spacing, but to image the entire state of California at a regional scale, to reveal some features that are difficult to resolve in local studies, and to provide the geophysical community with a velocity model that should be useful for regional-scale studies, such as regional waveform modeling. The model is available in the  electronic edition of *BSSA*.

Conclusions

We have developed statewide body-wave tomography models (P and S) for California using absolute and differential arrival times from earthquakes, controlled sources, and quarry blasts. By merging the data sets from networks in northern, southern, and coastal central California and USArray, we have achieved relatively complete coverage of the entire state for V_P . By including a large amount of active-source data in this study, we obtained improved resolution in near-surface layers over the previous California tomographic models, especially in the largest sedimentary basins, such as the Great Valley, the Imperial Valley, and the Los Angeles basin. At 8 km depth, there is a clear north to south increase in the average velocity of the Coast Range Mountains extending from the Mendocino Triple Junction to the border with Mexico. At 14 and 20 km depths, the basin and valley areas show relatively high-velocity anomalies, with lower velocities present under the mountain ranges. The Great Valley ophiolite body and the subducting Gorda Plate are evident from the cross sections. Low-velocity anomalies in the Sierra Nevada exist from midcrustal to greater depths; the slow velocity root over this area is the largest anomaly at 35 km depth. Our model provides a reasonable fit to the data and relocates explosions, treated as earthquakes, with an absolute accuracy of better than a kilometer. Thus, it should be useful for producing a statewide earthquake location catalog based on a single velocity model.

Data and Resources

Active-source data used in this study were collected from published studies listed in the references. Catalog picks were obtained from the USArray, the Northern California Earthquake Data Center (NCEDC), and the Southern California Earthquake Data Center (SCEDC) and originate principally from the Northern California Seismic Network (NCSN) and Southern California Seismic Network (SCSN). Some figures were made using the public domain Generic Mapping Tools software (Wessel and Smith, 1991).

Acknowledgments

We thank the U.S. Geological Survey (USGS) and Caltech staff for maintaining the NCSN and SCSN, and the IRIS Data Management Center for making USArray data available. R. Catchings, C. Evangelidis, A. Frankel, G. Fuis, S. Hartzell, W. Kohler, A. Lindh, J. Murphy, D. O'Connell, and T. Parsons contributed first-arrival times and receiver and source locations for active-source experiments in the study area. We thank W.-X. Du for his effort to assemble the northern California active-source data set into a consistent form and Y. Yang for providing his ambient noise tomography model. This work is supported by the National Earthquake Hazards Reduction program, under USGS awards 07HQGR0038, 07HQGR0045, 07HQGR0047, 07HQGR0050, 08HQGR0032, 08HQGR0039, 08HQGR0042 and 08HQGR0045, and the National Mapping Programs of the USGS. The views and conclusions contained in this document are those of the authors and should not be interpreted as necessarily representing the official policies, either expressed or implied, of the U.S. government.

References

- Begnaud, M. L., K. C. McNally, D. S. Stakes, and V. A. Gallardo (2000). A crustal velocity model for locating earthquakes in Monterey Bay, California, *Bull. Seismol. Soc. Am.* **90**, 1391–1408, doi [10.1785/B0120000016](https://doi.org/10.1785/B0120000016).
- Bleibinhaus, F., J. A. Hole, T. Ryberg, and G. S. Fuis (2007). Structure of the California Coast Ranges and San Andreas Fault at SAFOD from seismic waveform inversion and reflection imaging, *J. Geophys. Res.* **112**, B06315, doi [10.1029/2006JB004611](https://doi.org/10.1029/2006JB004611).
- Boyd, O. S., C. H. Jones, and A. F. Sheehan (2004). Foundering lithosphere imaged beneath the southern Sierra Nevada, California, USA, *Science* **305**, 660–662.
- Brocher, T. M. (2005). Empirical relations between elastic wavespeeds and density in the Earth's crust, *Bull. Seismol. Soc. Am.* **95**, 2081–2092.
- Brocher, T. M., and D. C. Pope (1994). Onshore-offshore wide-angle seismic recordings of the San Francisco Bay Area Seismic Imaging eXperiment (BASIX); data from the Northern California Seismic Network, *U.S. Geol. Surv. Open-File Rept.* 94-156.
- Brocher, T. M., P. E. Hart, and S. Carle (1989). Feasibility study of the seismic reflection method in Amargosa Desert, Nye County, Nevada, *U.S. Geol. Surv. Open-File Rept.* 89-133, 150 pp.
- Brocher, T. M., M. J. Moses, and S. D. Lewis (1992). Wide-angle seismic recordings obtained during seismic reflection profiling by the S. P. Lee offshore the Loma Prieta epicenter, *U.S. Geol. Surv. Open-File Rept.* 92-245, 63 pp.
- Catchings, R. D., M. R. Goldman, C. E. Steedman, and G. Gandhok (2004). Velocity models, first-arrival travel times, and geometries of 1991 and 1993 USGS land-based controlled-source seismic investigations in the San Francisco Bay Area, California: In-line Shots, *U.S. Geol. Surv. Open-File Rept.*, 2004-1423, 32 pp.
- Colburn, R. H., and W. D. Mooney (1986). Two-dimensional velocity structure along the synclinal axis of the Great Valley, California, *Bull. Seismol. Soc. Am.* **76**, 1305–1322.
- Colburn, R. H., and A. W. Walter (1984). Data report for two seismic-refraction profiles crossing the epicentral region of the 1983 Coalinga, California earthquakes, *U.S. Geol. Surv. Open-File Rept.* 84-643, 58 pp.
- Eberhart-Phillips, D. (1986). Three-dimensional velocity structure in the northern California Coast Ranges from inversion of local earthquake arrival times, *Bull. Seismol. Soc. Am.* **76**, 1025–1052.
- Eberhart-Phillips, D. (1990). Three-dimensional P and S velocity structure in the Coalinga region, California, *J. Geophys. Res.* **95**, 15,343–15,363.
- Eberhart-Phillips, D. (1993). Local earthquake tomography: earthquake source regions, in *Seismic Tomography: Theory and Practice*, H. M. Iyer and K. Hirahara (Editors), Chapman and Hall, London, 613–643.
- Eberhart-Phillips, D., and A. J. Michael (1993). Three-dimensional velocity structure, seismicity, and fault structure in the Parkfield region, central California, *J. Geophys. Res.* **98**, 15737–15758.
- Eberhart-Phillips, D., and A. J. Michael (1998). Seismotectonics of the Loma Prieta, California, region determined from three-dimensional V_p , V_p/V_s , and seismicity, *J. Geophys. Res.* **103**, 21,099–21,120.
- Evans, J. R., D. Eberhart-Phillips, and C. H. Thurber (1994). User's manual for SIMULPS12 for imaging V_p and V_p/V_s : A derivative of the "Thurber" tomographic inversion SIMUL3 for local earthquakes and explosions, *U.S. Geol. Surv. Open-File Rept.* 94-431.
- Flanagan, M. P., S. C. Myers, and K. D. Koper (2007). Regional travel-time uncertainty and seismic location improvement using a three-dimensional *a priori* velocity model, *Bull. Seismol. Soc. Am.* **97**, 804–825.
- Fliedner, M. M., S. L. Klemperer, and N. I. Christensen (2000). Three-dimensional seismic model of the Sierra Nevada arc, California, and its implications for crustal and upper mantle composition, *J. Geophys. Res.* **105**, 10899–10922.
- Fliedner, M. M., S. Ruppert, and the Southern Sierra Nevada Continental Dynamics Working Group (1996). Three-dimensional crustal structure of the southern Sierra Nevada from seismic fan profiles and gravity modeling, *Geology* **24**, 367–370.
- Foxall, W., A. Michelini, and T. V. McEvilly (1993). Earthquake travel time tomography of the southern Santa Cruz Mountains: Control of fault rupture by lithological heterogeneity of the San Andreas Fault zone, *J. Geophys. Res.* **98**, 17,691–17,710.
- Fuis, G., and W. D. Mooney (1990). Lithospheric structure and tectonics from seismic-refraction and other data, *The San Andreas Fault System, California: U.S. Geol. Surv. Prof. Paper* 1515, 207–236.
- Fuis, G. S., W. D. Mooney, J. H. Healy, G. A. McMechan, and W. J. Lutter (1984). A seismic refraction survey of the Imperial Valley region, California, *J. Geophys. Res.* **89**, 1165–1190.
- Fuis, G. S., J. M. Murphy, D. A. Okaya, R. W. Clayton, P. M. Davis, K. Thygesen, S. A. Baher, T. Ryberg, M. L. Benthien, G. Simila, J. T. Perron, A. K. Yong, L. Reusser, W. J. Lutter, G. Kaip, M. D. Fort, I. Asudeh, R. Sell, J. R. Vanschaack, E. E. Criley, R. Kaderabek, W. M. Kohler, and N. H. Magnuski (2001). Report for borehole explosion data acquired in the 1999 Los Angeles region seismic experiment (LARSE II), southern California. I. Description of the survey, *U.S. Geol. Surv. Open-File Rept.* 01-408, 82 pp.
- Fuis, G. S., T. Ryberg, N. J. Godfrey, D. A. Okaya, and J. M. Murphy (2001b). Crustal structure and tectonics from the Los Angeles basin to the Mojave Desert, southern California, *Geology* **29**, 15–18.
- Fuis, G. S., T. Ryberg, N. J. Godfrey, D. A. Okaya, W. J. Lutter, J. M. Murphy, and V. E. Langenheim (2000). Crustal structure and tectonics of the San Andreas Fault in the Central Transverse Ranges/Mojave Desert Area, *3rd Conference on Tectonic Problems of the San Andreas Fault System*.
- Fuis, G. S., J. J. Zucca, W. D. Mooney, and B. Milkereit (1987). A geologic interpretation of seismic-refraction results in northeastern California, *Geol. Soc. Am. Bull.* **98**, 53–65.
- Godfrey, N. J., B. C. Beaudoin, and S. L. Klemperer (1997). Ophiolitic basement to the Great Valley forearc basin, California, from seismic and gravity data: Implications for crustal growth at the North American continental margin, *Geol. Soc. Am. Bull.* **109**, 1536–1562.

- Hardebeck, J. L., A. J. Michael, and T. M. Brocher (2007). Seismic velocity structure and seismotectonics of the eastern San Francisco Bay region, California, *Bull. Seismol. Soc. Am.* **97**, 826–842.
- Harris, R., A. W. Walter, and G. S. Fuis (1988). Data report for the 1980–1981 seismic-refraction profiles in the western Mojave Desert, California, *U.S. Geol. Surv. Open-File Rept.* 88-580, 65 pp.
- Hauksson, E. (2000). Crustal structure and seismicity distribution adjacent to the Pacific and North America plate boundary in southern California, *J. Geophys. Res.* **105**, 13,875–13,903.
- Hauksson, E., and J. S. Haase (1997). Three-dimensional V_p and V_p/V_s velocity models of the Los Angeles basin and central Transverse Ranges, California, *J. Geophys. Res.* **102**, 5423–5453.
- Hauksson, E., and J. Unruh (2007). Regional tectonics of the Coso geothermal area along the intracontinental plate boundary in central eastern California: Three-dimensional V_p and V_p/V_s models, spatial-temporal seismicity patterns, and seismogenic deformation, *J. Geophys. Res.* **112**, B06309, doi10.1029/2006JB004721.
- Hellweg, M., D. Given, E. Hauksson, D. Neuhauser, D. Oppenheimer, and A. Shakal (2007). The California Integrated Seismic Network, *Eos Trans. AGU* **88**, Jt. Assem. Suppl., Abstract S33C-07.
- Henstock, T. J., A. Levander, and J. A. Hole (1997). Deformation in the lower crust of the San Andreas Fault System in northern California, *Science* **278**, 650–653.
- Holbrook, W. S., T. M. Brocher, U. S. ten Brink, and J. A. Hole (1996). Crustal structure of a transform plate boundary: San Francisco Bay and the central California continental margin, *J. Geophys. Res.* **101**, 22,311–22,334.
- Hole, J. A., T. Ryberg, G. S. Fuis, F. Bleibinhaus, and A. K. Sharma (2006). Structure of the San Andreas Fault zone at SAFOD from a seismic refraction survey, *Geophys. Res. Lett.* **33**, doi 10.1029/2005GL025194.
- Huang, J.-I., and D. Zhao (2003). P -wave tomography of crust and upper mantle under southern California: Influence of topography of Moho discontinuity, *Acta Seismologica Sinica* **16**, 577–587.
- Hwang, L. J., and W. D. Mooney (1986). Velocity and Q structure of the Great Valley, California, based on synthetic seismogram modeling of seismic refraction data, *Bull. Seismol. Soc. Am.* **76**, 1053–1067.
- Jachens, R. C., A. Griscom, and C. W. Roberts (1995). Regional extent of Great Valley basement west of the Great Valley, California: Implications for extensive tectonic wedging in the California Coast Ranges, *J. Geophys. Res.* **100**, 12,769–12,790.
- Kohler, W. M., and R. D. Catchings (1994). Data report for the 1993 seismic refraction experiment in the San Francisco Bay Area, California, *U.S. Geol. Surv. Open-File Rept.* 94-241, 71 pp.
- Kohler, W. M., and G. S. Fuis (1988). Data report for the 1979 seismic-refraction experiment in the Imperial Valley region, California, *U.S. Geol. Surv. Open-File Rept.* 88-255, 96 pp.
- Kohler, W. M., G. S. Fuis, and P. A. Berge (1987). Data report for the 1978–1985 seismic-refraction surveys in northeastern California, *U.S. Geol. Surv. Open-File Rept.* 87-625, 99 pp.
- Lin, G., P. M. Shearer, E. Hauksson, and C. H. Thurber (2007). A three-dimensional crustal seismic velocity model for southern California from a composite event method, *J. Geophys. Res.* **112**, doi 10.1029/2007JB004977.
- Luetgert, J. H., and W. D. Mooney (1985). Crustal refraction profile of the Long Valley caldera, California, from the January 1983 Mammoth Lakes earthquake swarm, *Bull. Seismol. Soc. Am.* **75**, 211–221.
- Lutter, W. J., G. S. Fuis, T. Ryberg, D. A. Okaya, R. W. Clayton, P. M. Davis, C. Prodehl, J. M. Murphy, V. E. Langenheim, M. L. Benthien, N. J. Godfrey, N. I. Christensen, K. Thygesen, C. H. Thurber, G. Simila, and G. R. Keller (2004). Upper crustal structure from the Santa Monica Mountains to the Sierra Nevada, Southern California: Tomographic results from the Los Angeles regional seismic experiment, phase II (LARSE II), *Bull. Seismol. Soc. Am.* **94**, 619–632.
- Lutter, W. J., G. S. Fuis, C. H. Thurber, and J. Murphy (1999). Tomographic images of the upper crust from the Los Angeles basin to the Mojave Desert, California: Results from the Los Angeles Region Seismic Experiment, *J. Geophys. Res.* **104**, 25,543–25,565.
- Magistrale, H., S. Day, R. W. Clayton, and R. Graves (2000). The SCEC southern California reference three-dimensional seismic velocity model version 2, *Bull. Seismol. Soc. Am.* **90**, S65–S76.
- Magistrale, H., K. McLaughlin, and S. Day (1996). A geology-based 3D velocity model of the Los Angeles basin sediments, *Bull. Seismol. Soc. Am.* **86**, 1161–1166.
- Manaker, D. M., A. J. Michael, and R. Burgmann (2005). Subsurface structure and kinematics of the Calaveras–Hayward Fault stepover from three-dimensional V_p and seismicity, San Francisco Bay region, California, *Bull. Seismol. Soc. Am.* **95**, 446–470.
- McMechan, G. A., and W. D. Mooney (1980). Asymptotic ray theory and synthetic seismograms for laterally varying structures: Theory and application to the Imperial Valley, California, *Bull. Seismol. Soc. Am.* **70**, 2021–2035.
- Meador, P. J., D. P. Hill, and J. H. Luetgert (1985). Data report for the July–August 1983 seismic-refraction experiment in the Mono Craters–Long Valley region, California, *U.S. Geol. Surv. Open-File Rept.* 85-708, 70 pp.
- Meltzer, A. S., A. R. Levander, and W. D. Mooney (1987). Upper crustal structure, Livermore Valley and vicinity, California coast ranges, *Bull. Seismol. Soc. Am.* **77**, 1655–1673.
- Mooney, W. D., and R. H. Colburn (1985). A seismic-refraction profile across the San Andreas, Sargent, and Calaveras faults, west-central California, *Bull. Seismol. Soc. Am.* **75**, 175–191.
- Mooney, W. D., and J. H. Luetgert (1982). A seismic refraction study of the Santa Clara Valley and southern Santa Cruz Mountains, west-central California, *Bull. Seismol. Soc. Am.* **72**, 901–909.
- Mooney, W. D., and C. S. Weaver (1989). Regional crustal structure and tectonics of the Pacific coastal states; California, Oregon and Washington, in *Geophysical Framework of the Continental United States*, I. C. Pakiser and W. D. Mooney (Editors), *Geol. Soc. Am. Mem.*, **172**, 129–161.
- Murphy, J. M. (1989). Data report for the Great Valley, California, axial seismic refraction profiles, *U.S. Geol. Surv. Open-File Rept.* 89-494, 36 pp.
- Murphy, J. M., and A. W. Walter (1984). Data report for a seismic-refraction investigation: Morro Bay to the Sierra Nevada, California, *U.S. Geol. Surv. Open-File Rept.* 84-642, 37 pp.
- Murphy, J. M., R. D. Catchings, W. M. Kohler, G. S. Fuis, and D. Eberhart-Phillips (1992). Data report for 1991 active-source seismic profiles in the San Francisco Bay area, *U.S. Geol. Surv. Open-File Rept.* 92-570, 45 pp.
- Murphy, J. M., G. S. Fuis, T. Ryberg, D. A. Okaya, E. E. Criley, M. L. Benthien, M. Alvarez, I. Asudeh, W. M. Kohler, G. N. Glassmoyer, M. C. Robertson, and J. Bhowmik (1996). Report for explosion data acquired in the 1994 Los Angeles Region Seismic Experiment (LARSE 94), Los Angeles, California, *U.S. Geol. Surv. Open-File Rept.* 96-536, 120 pp.
- Ryberg, T., and G. S. Fuis (1998). The San Gabriel Mountains bright reflective zone: Possible evidence of young mid-crustal thrust faulting in southern California, *Tectonophysics* **286**, 31–46.
- Sharpless, S. W., and A. W. Walter (1988). Data report for the 1986 San Luis Obispo, California, seismic refraction survey, *U.S. Geol. Surv. Open-File Rept.* 88-35, 48 pp.
- Spieth, M. A., D. P. Hill, and R. J. Geller (1981). Crustal structure in the northwestern foothills of the Sierra Nevada from seismic refraction experiments, *Bull. Seismol. Soc. Am.* **71**, 1075–1087.
- Steppe, A. J., and C. S. Robert (1978). P -velocity models of the southern Diablo Range, California, from inversion of earthquake and explosion arrival times, *Bull. Seismol. Soc. Am.* **68**, 357–367.
- Thurber, C. H. (1983). Earthquake locations and three-dimensional crustal structure in the Coyote Lake area, central California, *J. Geophys. Res.* **88**, 8226–8236.
- Thurber, C. H. (1993). Local earthquake tomography: Velocities and V_p/V_s -theory, in *Seismic Tomography: Theory and Practice*,

- H. M. Iyer and K. Hirahara (Editors), Chapman and Hall, London, 563–583.
- Thurber, C. H., S. R. Atre, and D. Eberhart-Phillips (1995). Three-dimensional V_p and V_p/V_s structure at Loma Prieta, California, from local earthquake tomography, *Geophys. Res. Lett.* **22**, 3079–3082.
- Thurber, C. H., T. M. Brocher, H. Zhang, and V. E. Langenheim (2007). Three-dimensional P wave velocity model for the San Francisco Bay region, California, *J. Geophys. Res.* **112**, doi [10.1029/2006JB004682](https://doi.org/10.1029/2006JB004682).
- Thurber, C., and D. Eberhart-Phillips (1999). Local earthquake tomography with flexible gridding, *Comp. Geosci.* **25**, 809–818.
- Thurber, C., S. Roecker, K. Robers, M. Gold, L. Powell, and K. Rittger (2003). Earthquake locations and three-dimensional fault zone structure along the creeping section of the San Andreas Fault near Parkfield, CA: Preparing for SAFOD, *Geophys. Res. Lett.* **30**, 1112, doi [10.1029/2002GL016004](https://doi.org/10.1029/2002GL016004).
- Thurber, C., S. Roecker, H. Zhang, S. Baher, and W. Ellsworth (2004). Fine-scale structure of the San Andreas Fault zone and location of the SAFOD target earthquakes, *Geophys. Res. Lett.* **31**, doi [10.1029/2003GL019398](https://doi.org/10.1029/2003GL019398).
- Thurber, C., H. Zhang, T. Brocher, and V. E. Langenheim (2009). Regional three-dimensional seismic velocity model of the crust and uppermost mantle of northern California, *J. Geophys. Res.* **114**, B01304, doi [10.1029/2008JB005766](https://doi.org/10.1029/2008JB005766).
- Thurber, C. H., H. Zhang, F. Waldhauser, J. Hardebeck, A. Michael, and D. Eberhart-Phillips (2006). Three-dimensional compressional wavespeed model, earthquake relocations, and focal mechanisms for the Parkfield, California, region, *Bull. Seismol. Soc. Am.* **96**, S38–S49.
- Waldhauser, F., and W. L. Ellsworth (2000). A double-difference earthquake location algorithm: Method and application to the Northern Hayward Fault, California, *Bull. Seismol. Soc. Am.* **90**, 1353–1368.
- Walter, A. W., and W. D. Mooney (1982). Crustal structure of the Diablo and Gabilan Ranges, central California: A reinterpretation of existing data, *Bull. Seismol. Soc. Am.* **72**, 1567–1590.
- Warren, D. (1978). Record sections for two seismic refraction profiles in the Gabilan and Diablo Ranges, California, *U.S. Geol. Surv. Open-File Rept. 78-340*, 95 pp.
- Warren, D. H. (1981). Seismic-refraction measurements of crustal structure near Santa Rosa and Ukiah, California, in *Research in the Geysers–Clear Lake geothermal area, northern California*, *U.S. Geol. Surv. Prof. Pap. 1141*, 167–181.
- Wessel, P., and W. H. F. Smith (1991). Free software helps map and display data, *Eos Trans. AGU* **72**, 441.
- Williams, A. J., T. M. Brocher, W. D. Mooney, and A. Boken (1999). Data report for seismic refraction surveys conducted from 1980 to 1982 in the Livermore Valley and the Santa Cruz Mountains, California, *U.S. Geol. Surv. Open-File Rept. 99-146*, 78 pp.
- Yang, Y., M. H. Ritzwoller, F.-C. Lin, M. Moschetti, and N. M. Shapiro (2008). Structure of the crust and uppermost mantle beneath the western United States revealed by ambient noise and earthquake tomography, *J. Geophys. Res.* **113**, B12310, doi [10.1029/2008JB005833](https://doi.org/10.1029/2008JB005833).
- Zhang, H., and C. Thurber (2006). Development and applications of double-difference seismic tomography, *Pure Appl. Geophys.* **163**, 373–403.
- Zhang, H., and C. H. Thurber (2003). Double-difference tomography: The method and its application to the Hayward Fault, California, *Bull. Seismol. Soc. Am.* **93**, 1875–1889.
- Zhang, H., and C. H. Thurber (2007). Estimating the model resolution matrix for large seismic tomography problems based on Lanczos bidiagonalization with partial reorthogonalization, *Geophys. J. Int.* **170**, 337–345.
- Zhou, H.-W. (2004). Multi-scale tomography for crustal P and S velocities in southern California, *Pure Appl. Geophys.* **161**, 283–302.
- Zucca, J. J., G. S. Fuis, B. Milkereit, W. D. Mooney, and R. D. Catchings (1986). Crustal structure of northeastern California, *J. Geophys. Res.* **91**, 7359–7382.

Department of Geoscience
University of Wisconsin–Madison
1215 W. Dayton St.
Madison, Wisconsin 53706
(G.L., C.H.T.)

Department of Earth, Atmospheric, and Planetary Sciences
Massachusetts Institute of Technology
77 Massachusetts Avenue, 54-1818
Cambridge, Massachusetts 02139
(H.Z.)

Seismological Laboratory
California Institute of Technology
1200 E. California Boulevard
Mail Code 252–21
Pasadena, California 91125
(E.H.)

Institute of Geophysics and Planetary Physics
Scripps Institution of Oceanography
University of California, San Diego
La Jolla, California 92093–0225
(P.M.S.)

Lamont-Doherty Earth Observatory
Columbia University
Palisades, New York 10964
(F.W.)

U.S. Geological Survey
345 Middlefield Road, MS 977
Menlo Park, California 94025
(T.M.B., J.H.)